EurJIC European Journal of Inorganic Chemistry

ChemPubSoc Europe

FULL PAPER

DOI:10.1002/ejic.201402614

Effect of the Metal Ion on the anti *T. cruzi* Activity and Mechanism of Action of 5-Nitrofuryl-Containing Thiosemicarbazone Metal Complexes

CLUSTER ISSUE

Micaella Cipriani,[a][‡] Jeannette Toloza,[b][‡] Lara Bradford,[a] Eugenia Putzu,[a] Marisol Vieites,[a] Estela Curbelo,[a] Ana Isabel Tomaz,[c] Beatriz Garat,[d] Juan Guerrero,[e] Jorge S. Gancheff,[a] Juan Diego Maya,[f] Claudio Olea Azar,[b] Dinorah Gambino,[a] and Lucía Otero*[a]

Keywords: Palladium / Platinum / Drug design / *Trypanosoma cruzi* / DNA

Chagas disease, caused by the protozoan parasite *Trypanosoma cruzi*, is a major health problem worldwide. In this work, we report the development of palladium and platinum metal complexes with 5-nitrofuryl-containing thiosemicarbazones (L) as bioactive ligands against *T. cruzi* and PTA (1,3,5-triaza-7-phosphaadamantane) as co-ligand. Eight new complexes of the formula [MCl(L)(PTA)] with M = Pd or Pt were synthesized and fully characterized. Most complexes showed similar activities against *T. cruzi* to those of the corresponding free thiosemicarbazone ligands. No significant differences between palladium and platinum complexes were observed. Metal compounds with the phenylthiosemicarbazone derivative were the most active ones ($IC_{50} = 9.84 \pm 0.32$ and 4.94 ± 0.24 μM for Pd^{2+} and Pt^{2+}, respectively). The prepared complexes were not toxic on mammalian cells, showing selective indexes of more than 10–20. The ability of the complexes to be reduced in the parasite, which leads to toxic free radical species, was confirmed by the detection of $OH^{\cdot}$ and nitroanion free radical species by ESR spectroscopy experiments. Gel electrophoresis and fluorescence experiments were consistent with an intercalating-like mode of DNA interaction for the complexes, but DNA interaction does not seem to be the main mechanism of anti *T. cruzi* action for these compounds. The results obtained show that complexation of the bioactive ligands with the selected metals is a valid strategy to obtain improved metal-based antiparasitic compounds.

Introduction

Inorganic compounds have been used to treat various diseases for many centuries. However, the development of modern coordination chemistry as well as the discovery of the antitumor activity of the inorganic complex *cis*-diamminedichloroplatinum(II) (cisplatin) in 1965 have made a major contribution to the development of modern inorganic medicinal chemistry. In fact, this area of inorganic chemistry has evolved from the serendipitous discovery of the pharmacological activity of different metal compounds towards the rational design of metal-based drugs having specific activities and molecular targets.[1–4] Metal complexes provide an ideal drug design platform, since many metal centers in different oxidation states could be used, different geometries could be obtained, and various ligands could be included in one species, which enables the modulation of biological activity and physicochemical properties, among other advantages.[3,4]

The most important progresses in the area of metal-based drugs have been made in the field of cancer therapy, and studies on platinum have led the work in this area, mainly focusing on its DNA-binding ability.[1] Because palladium has a very similar chemistry to that of platinum, many analogous potential antitumor Pt^{II} and Pd^{II} complexes have also been developed. Both metal ions form square-planar complexes, and they are soft Lewis acids pre-

[a] Cátedra de Química Inorgánica, Facultad de Química, UdelaR, Gral Flores 2124, Montevideo, Uruguay
E-mail: luotero@fq.edu.uy
gqim.fq.edu.uy
[b] Departamento de Química Inorgánica y Analítica, Facultad de Ciencias Químicas y Farmacéuticas, Universidad de Chile, Santiago, Chile
[c] Centro de Ciências Moleculares e Materiais, Faculdade de Ciências, Universidade de Lisboa, 1749-016 Lisboa, Portugal
[d] Laboratorio de Interacciones Moleculares, Facultad de Ciencias, UdelaR, Montevideo, Uruguay
[e] Departamento de Ciencias de los Materiales, Facultad de Química y Biología, Universidad de Santiago de Chile, Avda. Bernardo O'Higgins 3363, Santiago, Chile
[f] Programa de Farmacología Molecular y Clínica, ICBM, Facultad de Medicina, Universidad de Chile, Santiago, Chile
[‡] Both authors contributed to this manuscript equally.
Supporting information for this article is available on the WWW under http://dx.doi.org/10.1002/ejic.201402614.

ferring nitrogen or sulfur donor ligands (soft bases). But, in general, Pt^{II} complexes are thermodynamically and kinetically more stable than those of Pd^{II}, which explains the lower activity and higher toxicity found for the latter. However, some palladium *S*,*N*-stable chelates have shown very promising results as antitumor agents, with DNA as their main target.[5]

Metal-based drugs have also become a promising alternative to find a pharmacological answer to tropical parasitic diseases.[6–11] These illnesses constitute a major world health problem, and they actually need more effective and less toxic drugs for their treatment as they have historically received low investment by the pharmaceutical industry.[12–14] In particular, the Chagas disease is an endemic illness that affects 7–8 million people worldwide. This disease is caused by a flagellated protozoan parasite, *Trypanosoma cruzi* (*T. cruzi*), and it is transmitted to humans by a blood-sucking insect of the *Triatominae* family (called vinchuca), which carries the parasite in its contaminated faeces. About one-third of all acute cases of the Chagas disease develop the chronic form, suffering from irreversible damage to the heart, oesophagus, and/or colon. The two drugs that are available for the treatment of this illness, nifurtimox and benznidazole, have no activity on the chronic phase, so patients with severe chronic disease become progressively more ill and finally die, usually from their heart condition.[15,16]

In the search of a pharmacological answer to the Chagas disease, our group has been working on the development of metal-based antichagasic drugs. One of our strategies has been the complexation of ligands bearing anti *T. cruzi* activity with pharmacologically active transition metals ions. The aim of this work has been the generation of agents that could modulate multiple targets: those related to the bioactive ligands and those related to the metal. In this way, we pretend to obtain new species with an improved chemical and pharmacological profile.[6,7,8–11] In particular, we have developed more than fifty palladium(II), platinum(II), and ruthenium(II) coordination and organometallic compounds with antichagasic 5-nitrofuryl-containing thiosemicarbazones (Figure 1) as ligands. The complexes have been rationally designed by including, in the coordination sphere of the metal ion, different co-ligands that could modulate the physicochemical properties of the designed complexes. Most complexes were demonstrated to be more active than or at least as active as the corresponding ligands, and the activity could be correlated to properties like solubility, stability, lipophilicity, or protein interaction. Compound mechanisms of anti *T. cruzi* action have been also extensively studied.[11,17–27]

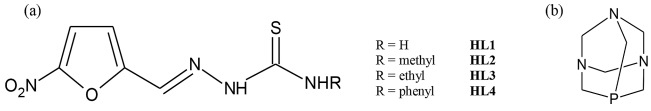

Figure 1. (a) 5-nitrofuryl-containing thiosemicarbazones, (b) PTA (1,3,5-triaza-7-phosphaadamantane).

On the basis of these results, we are now reporting the development of Pd^{II} and Pt^{II} complexes with 5-nitrofuryl-containing thiosemicarbazones (L, Figure 1) as bioactive ligands and the hydrophilic phosphine PTA (1,3,5-triaza-7-phosphaadamantane, Figure 1) as co-ligand. The effect of the metal ion and the co-ligand on the chemical and biological properties of the prepared species was studied. Palladium and platinum were selected on the basis of the similarities between metabolic pathways of highly proliferative cells, like parasites and tumor cells, that have led to a correlation between antiparasitic and antitumor activities.[8,28] In this sense, DNA could be a potential parasitic target for these compounds. PTA was included in order to modulate the solubility and lipophilicity of the complexes. In addition, this ligand has been reported to favor DNA interaction as a consequence of *N*-protonation under some physiological conditions.[29,30] Two potential mechanisms of action could be expected for the complexes due to the bioactive thiosemicarbazone ligands: production of reduced oxygen species (ROS) that cause parasite damage,[31] and inhibition of cruzipain, the main *T. cruzi* cysteine protease.[32]

In this work, the synthesis, complete characterization (including theoretical calculations), the in vitro anti *T. cruzi* activity, and the potential mechanism of action (ROS production, cruzipain inhibition, and DNA interaction) of eight new M–PTA–L complexes with M = Pd or Pt are reported. A comparative study of the effect of the metal ion on the biological activity and the mechanism of action of the Pd and Pt species along with that of the previously reported Ru–PTA–L[23] complexes was performed.

Results and Discussion

Synthesis and Characterization

Eight new analogous palladium(II) and platinum(II) neutral complexes of formula [MCl(L)(PTA)] were prepared in good yield and high purity from the corresponding $[MCl_4]^{2-}$ salts. All analytical and spectroscopic characterizations are in agreement with the proposed formulae. Conductivity measurements performed in 1 mM DMSO solutions confirm the neutrality of the obtained complexes. Even though a molar excess of PTA ligands was used, coordination of two of these ligands could not be achieved maybe because of the high insolubility of the obtained neutral species. In fact, the palladium and platinum complexes were not soluble in water and in most common solvents. However, the previously reported $[RuCl_2(HL)(HPTA)_2]Cl_2$ complexes were very water soluble.[27] The presence of two PTA ligands in these complexes and/or their charge could explain such differences.

The infrared vibrational spectroscopic behavior of the eight metal complexes was studied in the solid state. All complexes showed a similar band pattern in accordance with analogous coordination structures. Significant bands of the FTIR spectra were tentatively assigned (aided by theoretical calculations, see below) in order to get infor-

mation about the coordination mode of the ligands. After coordination, clear changes in the wavenumber of the υ(C=N) and υ(N–N) bands of the free thiosemicarbazone ligands were observed. These modifications have been related to the coordination of the ligand through the imine nitrogen and to the electronic delocalization produced as a consequence of both coordination and deprotonation.[33] This last fact was also confirmed as the υ(NH) band, at approximately 3120–3150 cm^{-1}, is absent in all complexes indicating the loss of the N–H proton of the CH=N–NH moiety upon coordination. In addition, υ(C=S) bands at around 820–850 cm^{-1}, should shift to lower wavenumbers when thiosemicarbazones act as N,S bidentate ligands, but as it has been previously stated, they could not be unambiguously assigned for the complexes.[21,22,26,27,33] PTA bands were also observed and tentatively assigned in the obtained complexes (Table S1, Supporting Information). As expected, some of them were shifted as a consequence of coordination.[27,29,30,34]

^{1}H and $^{31}P\{^{1}H\}$ NMR spectroscopic experiments supported the proposed structures of the synthesized complexes. Two-dimensional NMR spectroscopic experiments, such as COSY and HSQC, aided in the assignment of the spectra. The ^{1}H NMR spectra of all complexes showed a similar pattern of signals for the common portions of the nitrofurylthiosemicarbazone ligands and PTA. Even though quite broad signals appeared in some of the obtained complexes, four signals corresponding to the two H atoms of the furan ring, C*H*=N, and N*H*-R protons of the thiosemicarbazone ligand are easily distinguishable. Upon coordination, the C*H*-N proton at around 8 ppm in the free ligands was significantly shifted downfield, which confirmed the coordination of the imine nitrogen to the metal center. The deshielding effect of platinum complexation is higher than that of palladium. In addition, in both the Pd^{2+} and Pt^{2+} complexes, this signal was observed as a doublet. This splitting is attributed to the coupling of the phosphorus nucleus of the PTA ligand to the nucleus of the imine proton four bonds away. This phenomenon has been previously reported for similar PTA complexes.[35,36] The absence of the signal corresponding to the CH=N–N*H* proton (around 11 ppm in the free ligands) is consistent with the coordination of the thiosemicarbazone ligand in a deprotonated form. The protons of the PTA ligands were observed in the region of 4.2–4.5 ppm.[30] The protons of the N–CH_2–N moiety present an AB spin system and appear as two doublets at around 4.4 and 4.5 ppm as a result of a diastereotopic behavior. The P–CH_2–N protons occur as a singlet in the region of 4.2 ppm for the palladium complexes and at 4.3 ppm (overlaid with one of the doublets) for the platinum complexes. This pattern is consistent with those observed for other PTA transition metal complexes.[35,36] The $^{31}P\{^{1}H\}$ NMR spectra showed only one signal at around –27 ppm for palladium complexes and at around –60 ppm for platinum complexes. In addition, for platinum complexes, two satellites at the sides of the phosphorus signal due to the coupling with platinum atom were observed.[37]

Geometry Optimization, Isomer Stability, and Vibrational IR Spectroscopy

The absence of crystallographic data prompted us to conduct stability studies of the two possible isomers arising from the different coordination positions of the chloride ligand: (1) the Cl–M–N isomer (in which the chloride is *trans* to the imine nitrogen) (2) the Cl–M–S isomer (in which the chloride is *trans* to the thiocarbonyl sulfur). The optimization for both isomers gives rise to a minimum as stationary point in all cases. The stability results are summed up in Table 1. The complex containing chloride *trans* to sulfur turned out to be the most stable one, regardless of the metal ion and the nature of R. The largest energy difference between isomers has been calculated for [PdCl(L)(PTA)] (11.1 kcal mol^{-1}). It may be worth pointing out that, for a given substituent R, platinum complexes have been computed as more stable than palladium complexes.

Table 1. B3LYP/LANL2DZ energies (in the gas phase) for different isomers of complexes [MCl(L)(PTA)] with two different coordination positions of chloride (T = 298 K).

M^{2+}	L	ΔE [kcal mol^{-1}] Cl–M–N[a,b]	ΔE [kcal mol^{-1}] Cl–M–S[a,b]
Pd^{2+}	L1	11.1	0
	L2	10.4	0
	L3	10.4	0
	L4	10.2	0
Pt^{2+}	L1	9.3	0
	L2	8.7	0
	L3	10.2	0
	L4	9.5	0

[a] Cl–M–N: isomer Cl–M–N; Cl–M–S: isomer Cl–M–S. [b] ΔE: energy difference with respect to the most stable isomer.

The use of PBE1PBE in combination with STMIDI (see Computational Details) has been successfully employed in studying electronic properties of large transition metal complexes with a very low computational cost.[38–42] In addition to the study of the electronic features of the title complexes, it is also our aim to test the reliability of PBE1PBE/STMIDI in studying the electronic properties of complexes with different metal ions bearing different donor atoms. Therefore, we decided to investigate the geometry and vibrational IR spectrum of complexes included in this work by employing PBE1PBE/STMIDI. Vibrational IR spectra (in the range 1750–500 cm^{-1}) of the isomers of [PtCl(L3)(PTA)] (taken as example) as calculated with PBE1PBE/STMIDI are displayed in Figure 2, which also exhibits the experimental spectrum.

The results displayed in Figure 2 reveal a very good agreement between the calculated spectrum for the Cl–Pt–S isomer and the experimental findings. A group of four absorption bands centered at about 1500 cm^{-1} has been detected. Their origin may be attributed to coupled stretching modes (of C–C and C–N bonds) with minor contributions from bending of the CH_2 group (ethyl substituent). Intense absorption bands in the range 1450–1300 cm^{-1} have also been observed. Stretching of the nitro substituent coupled with stretching of C–C, N–N, and C–H bonds can be con-

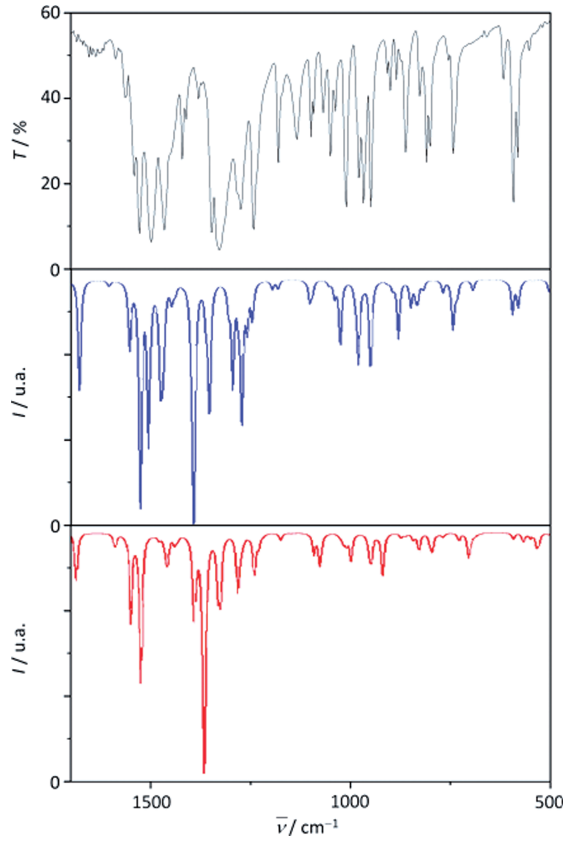

Figure 2. Vibrational IR spectra of complex [PtCl(L3)(PTA)]: experimental spectrum (top), and theoretical spectra as calculated with PBE1PBE/STMIDI for the isomers Cl–Pt–S (middle, blue line) and Cl–Pt–N (bottom, red line) (T = 298 K). Absorption bands only in the range from 500 to 1750 cm^{-1} are exhibited.

sidered as their origin. Combination modes of the PTA ligand are associated with three calculated bands at about 1000 cm^{-1} (1051, 1003, and 972 cm^{-1}). At the lowest-energy region of the spectrum, two bands (experimentally observed as intense) have been computed at 600 and 584 cm^{-1}, whose origin can be traced to coupled modes involving stretching of Pt–P and Pt–N bonds. The theoretical results already discussed allow us to assume that the title complexes are obtained as the Cl–M–S isomer in the solid state. With this in mind, we decided to explore the geometrical features of this isomer of complex [PtCl(L3)(PTA)] (Figure 3) with PBE1PBE/STMIDI. Selected optimized parameters are summed up in Table 2.

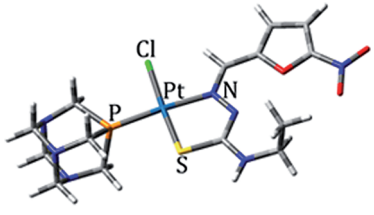

Figure 3. Optimized geometry of isomer Cl–Pt–S of complex [PtCl(L3)(PTA)] as obtained with PBE1PBE/STMIDI (T = 198 K).

The optimized structure of complex [PtCl(L3)(PTA)] displays the metal ion in a square-planar coordination geometry. Selected metric parameters reasonably match those observed in complexes of Pt^{2+} with a similar coordination environment.[43] While the optimized bond distance Pt–P is almost identical to that of complex [PtCl(N∩S**)-(PMe_2Ph)] (deviation of 0.01 Å),[43] the distance Pt–Cl is sensitive to the nature of the bidentate ligand and shows a deviation of 0.094 Å. The values of selected bond angles are also in line with the geometric features of complex [PtCl(N∩S**)(PMe_2Ph)].[43]

Table 2. Selected geometric parameters for the most stable isomer of complex [PtCl(L3)(PTA)] as calculated with PBE1PBE/STMIDI (T = 298 K).

Bond	d [Å]	Angle	∠ [°]
Pt–N	2.078	N–Pt–S	83.4
Pt–S	2.266	N–Pt–Cl	93.7
Pt–Cl	2.309	P–Pt–Cl	90.8
Pt–P	2.246	P–Pt–S	92.1
		N–Pt–P	175.5
		Cl–Pt–S	177.1

Cyclic Voltammetry Studies

All obtained compounds display similar voltammetric behavior in DMSO solution as measured by means of a hanging drop mercury working electrode. Ligand centered electrochemical processes for both PTA and thiosemicarbazone ligands can be observed when the potential is scanned in the negative direction. A well-defined quasi-reversible wave corresponding to a PTA centered reduction process appears at approximately –0.4 V (vs. Ag/Ag^+). This potential is lower than that of the free PTA as previously observed for other PTA metal complexes.[27] A second quasi-reversible wave at –1.1 V vs. Ag/Ag^+, related to the thiosemicarbazone ligand, can be assigned to a process involving a one-electron transfer, which leads to the generation of the anion radical $RNO_2^{\cdot-}$ by reduction of the nitro moiety. Other thiosemicarbazone-centered waves corresponding to further reduction of the nitro moiety and/or self-protonation processes have also been observed.[23,44]

It had been previously demonstrated that the first step of the mechanism of anti *T. cruzi* action of the 5-nitrofuryl-containing thiosemicarbazones involves the reduction of the nitro moiety. Through redox cycling, the nitro anion formed would generate other radical species that are toxic for the parasite.[31] In this regard, the redox potential of the nitro group could be a way of predicting how easy this reduction process could be in vivo. The peak potentials obtained are shown in Table 3. The reduction potentials of the nitro moiety decreased by about 0.1 V upon formation of the complexes. The nitro group of both palladium and platinum complexes is more easy to reduce than that of the free ligands. This positive influence of complexation could lead to an increased biological activity. In addition, the nitro moiety of these complexes is more easily reducible than that of the reference drug nifurtimox. On the other hand, for the previously obtained $[RuCl_2(HL)(HPTA)_2]Cl_2$ com-

plexes, the opposite effect was observed: the nitro group of the complexes was more difficult to reduce than that of the free thiosemicarbazone ligands. In that case, a decrease of the biological activity was observed.[27]

Table 3. Lipophilicity values and reduction potentials of the nitro moiety measured in DMSO solutions at 100 mV s^{-1} (vs. Ag/Ag$^+$ reference electrode).

Compound	Couple $RNO_2/RNO_2^{\cdot-}$		R_M[c]
	E_{pc}[a] [V]	E_{pa}[b] [V]	
HL1	–1.10	–1.00	–0.7
[PdCl(L1)(PTA)]	–1.01	–0.93	–0.5
[PtCl(L1)(PTA)]	–1.01	–0.95	–1.2
HL2	–1.09	–1.00	–0.6
[PdCl(L2)(PTA)]	–1.01	–0.95	–0.3
[PtCl(L2)(PTA)]	–0.97	–0.93	–0.6
HL3	–1.11	–1.02	–0.5
[PdCl(L3)(PTA)]	–1.01	–0.94	–0.1
[PtCl(L3)(PTA)]	–0.97	–0.87	–0.7
HL4	–1.07	–0.99	–0.1
[PdCl(L4)(PTA)]	–0.96	–0.89	0.1
[PtCl(L4)(PTA)]	–0.93	–0.85	–0.2
Nifurtimox	–1.17	–1.11	–

[a] Cathodic peak potential. [b] Anodic peak potential. [c] $R_M = \log[(1/R_f) - 1]$, elution mixture DMSO/physiological serum 60:40 (v/v).

Electron Spin Resonance Spectroscopy

To elucidate the potential mechanism of action of the obtained complexes, they were tested for their capability to produce free radicals under reductive conditions. The free radicals characterized by ESR spectroscopy were prepared in situ by electrochemical reduction in DMSO, by applying a potential corresponding to the monoelectronic wave of the nitro moiety obtained from the cyclic voltammetric experiments. All complexes formed stable paramagnetic species at that first reduction step that are stabilized due to the delocalization of the unpaired electron. The interpretation of the ESR spectra was performed by means of a simulation process using the hyperfine coupling constants (hfccs) previously obtained for the free thiosemicarbazone ligands, modifying the line width the modulation amplitude and the Lorentzian/Gaussian component.[44] The obtained hfccs are listed in Table 4. A representative ESR spectrum is shown in Figure 4. The ESR spectra of the radical species obtained were simulated in terms of three triplets corresponding to the nitrogen nucleus of the nitro group and two nitrogen nuclei of the CH=N–NH– moiety, and two doublets due to inequivalent hydrogen atoms belonging to the nitrofuran ring. For some of the complexes, another triplet corresponding to the terminal nitrogen nucleus, as well as two more doublets of the hydrogen atoms belonging to the thiosemicarbazone chain, had to be included in the simulation results (Table 4). The ESR spectrum of both [PtCl(L4)(PTA)] radicals showed a wide line with no pattern of hyperfine coupling, so hfccs would be smaller than the line width. For the rest of the complexes, the higher hfccs were obtained for the nucleus of the imine nitrogen coordinated to the metal ion, evidencing the electron-withdrawing effect of the metal.

Table 4. Hyperfine splittings [G] for the anion radical of the platinum and palladium complexes.[a]

Compound	aN1	aN2	αN3	aN4	aH1	aH2	αH3	aH4
[PtCl(L1)(PTA)]	3.06	6.12	2.59	3.04	3.52	3.13	3.08	2.56
[PtCl(L2)(PTA)]	2.70	5.93	2.61	–	3.90	2.96	–	–
[PtCl(L3)(PTA)]	3.71	6.63	2.79	–	4.88	2.50	–	–
[PdCl(L1)(PTA)]	1.11	8.45	1.17	0.63	3.66	4.89	0.33	0.36
[PdCl(L2)(PTA)]	0.52	6.89	5.19	–	3.97	2.55	–	–
[PdCl(L3)(PTA)]	2.99	8.77	3.00	–	1.50	2.50	0.75	0.66

[a] Nucleus numbering: $N1O_2$, CH=N2–N3 H, N4H–R, H1, and H2 of the nitrofuran ring, CH_3=N, NH_4–R.

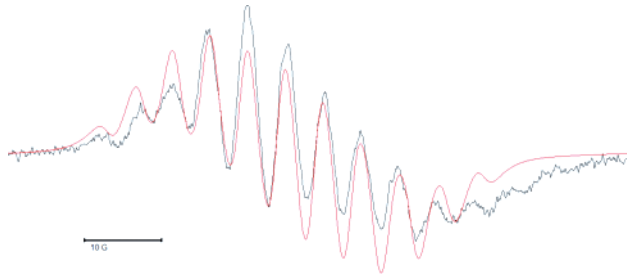

Figure 4. Experimental (black) and simulated (red) ESR spectra for the [PtCl(L1)(PTA)] radical. Spectrometer conditions: microwave frequency 9.68 Ghz, microwave power 20 mW, modulation amplitude 0.20 G. The spectrum was simulated by using the following parameter line width: 0.9 G, ratio Lorentzian/Gaussian 1.0.

Lipophilicity

The lipophilicity of the complexes was experimentally investigated by reverse-phase TLC in terms of R_M values. In such experiments, the stationary phase (precoated TLC-C18) may be considered to simulate lipids of biological membranes or receptors, and the mobile phase, (DMSO/physiological serum 60:40 v/v) resembles the aqueous biological milieu. The composition of the mobile phase was adjusted in order to enable complexes to be differentiated according to their lipophilicity.[21,27] The results are shown in Table 3. The effect of the different metal ions on the R_M values is evident. Palladium complexes are more lipophilic than the corresponding thiosemicarbazone ligands, while platinum complexes are less lipophilic. As expected, for each metal ion, the lipophilicity of the complexes increases as the *N*-substituent in the thiosemicarbazone ligand changes from H to phenyl. [Pd(L4)(PTA)] was the most lipophilic complex of the series. For the previously obtained $[RuCl_2(HL)(HPTA)_2]Cl_2$ compounds, the lipophilicity increased in spite of the presence of two hydrophilic PTA ligands in the complexes, all ruthenium complexes being more lipophilic than both palladium and platinum ones.[27]

Biological Results

The stability of the compounds in DMSO was studied by UV/Vis spectroscopy, conductivity measurements, and

^{1}H NMR spectroscopy. No observable decomposition was observed after 24 h.

In vitro Anti T. cruzi Activity

The data presented in Table 5 show the effects of the obtained palladium and platinum complexes and the corresponding ligands on the growth of the trypomastigote form of *T. cruzi* (Dm28c clone). Most complexes were as active as or less active than the corresponding ligands. However, both [MCl(L4)(PTA)] complexes were the most active (IC_{50} = 9.8 ± 0.3 and 4.9 ± 0.2 μM for Pd and Pt, respectively), being more active than the reference drug nifurtimox and the free phenylthiosemicarbazone derivative. Even when no important differences between the activity of palladium and platinum complexes were observed, the effect of the metal ion is evident when comparing these results with those of the previously reported $[RuCl_2(HL)(HPTA)_2]Cl_2$ complexes. Even the most active ruthenium complex was less active than any of the obtained palladium and platinum complexes.[27] No clear correlation between the lipophilicity values and the anti *T. cruzi* activity could be observed for any of the metal–PTA–L complexes. Indeed, the ruthenium complexes are the most lipophilic ones and they are also the less active.

Table 5. In vitro activity against *T. cruzi* trypomastigotes (Dm28c clone) and cytotoxicity toward EA.hy926 mammalian cells. The results are the mean values of three different experiments.

Compound	Anti *T. cruzi* activity		Cytotoxicity (EA.hy926)
	Viability [%] (10 μM)	IC_{50} [μM][b]	IC_{50} [μM]
HL1	43.0 ± 0.4	9.8 ± 1.5[a]	>100
[PdCl(L1)(PTA)]	70.5 ± 2.5	ND	86.8 ± 0.2
[PtCl(L1)(PTA)]	60.3 ± 2.4	58.0 ± 1.3	49.9 ± 2.5
HL2	48.5 ± 0.4	17.4 ± 1.9[a]	>100
[PdCl(L2)(PTA)]	57.0 ± 0.6	ND	29.8 ± 1.5
[PtCl(L2)(PTA)]	56.8 ± 1.0	13.0 ± 0.2	39.26 ± 1.53
HL3	36.1 ± 0.4	18.5 ± 1.7[a]	>100
[PdCl(L3)(PTA)]	53.9 ± 2.8	ND	45.8 ± 2.1
[PtCl(L3)(PTA)]	57.4 ± 2.6	41.2 ± 1.1	35.1 ± 1.6
HL4	59.0 ± 0.5	22.7 ± 1.6[a]	>100
[PdCl(L4)(PTA)]	49.8 ± 0.9	9.8 ± 0.3	>100
[PtCl(L4)(PTA)]	47.0 ± 1.9	4.9 ± 0.2	>100
Nifurtimox	–	20.1 ± 0.8[c]	–

[a] Data from ref.[17] [b] ND: not determined (because of solubility problems). [c] Data from ref.[27]

Cytotoxicity on EA.hy926 Mammalian Cells

The specificity of the antiparasitic activity of the obtained metal compounds and the thiosemicarbazone ligands was evaluated by analyzing their cytotoxicity against the endothelial cell line EA.hy926. The results are exhibited in Table 5. The most active anti *T. cruzi* complexes, that is, [MCl(L4)(PTA)], showed no toxicity on the assayed mammalian cell line. In fact, the selective indexes for these compounds were higher than 10 or 20 for palladium and platinum complexes, respectively.

Mechanism of Action

The metal complexes prepared were designed to show a dual or even a multiple mechanism of action by affecting different targets or biologically significant processes in the parasite. Accordingly, different studies were performed in order to validate the proposed targets and to get insight into the probable mechanism of action of the new metal compounds.

Production of Free Radicals in T. cruzi

The mechanism of anti *T. cruzi* action of other previously reported metal complexes with 5-nitrofuryl-containing thiosemicarbazones as ligands seems to remain the same as those of the free bioactive ligands.[17,16,22,23,26,27] This mechanism involves bioreduction and the production of toxic free radical species. In this line, compounds were incubated with *T. cruzi* (Dm28c strain) epimastigotes, and the production of free radicals was assessed by ESR spectroscopy. DMPO was added to the solutions in order to trap possible intracelullar free radical species having short half-lives. All palladium and platinum complexes showed a similar line pattern in the ESR spectra. As an example, the ESR spectrum for the [PtCl(L4)(PTA)] complex is shown in Figure 5.

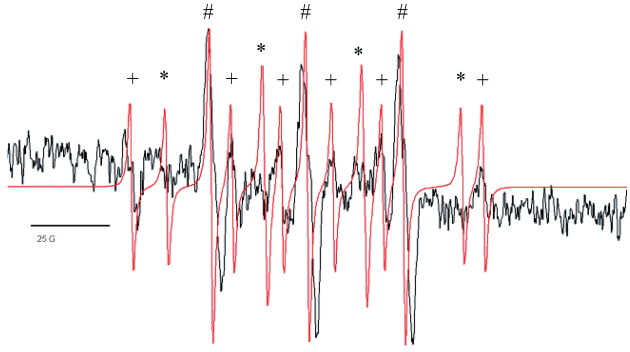

Figure 5. Experimental (black) and simulated (red) ESR spectra obtained after 5 min incubation of [PtCl(L4)(PTA)] (1 mM) with *T. cruzi* epimastigotes (Dm28c strain, final protein concentration 4–8 mg/mL), NADPH (1 mM), and DMPO (100 mM): (+) characteristic signals of the spin adduct of DMPO and the nitro compound. (*) characteristic signals of the DMPO–OH spin adduct. (#) DMPO or DMPO–OH oxidation signals.

A thirteen-line spectral pattern was observed, corresponding to three different DMPO spin adducts. A carbon-centered radical trapped by DMPO (+) with characteristic coupling constants of aN = 15.0 G and aH = 22.5 G could be related to the bioreduction of the complexes and the formation of DMPO–nitroheterocyclic radical species.[27,45] In addition, intracellular hydroxy radical was also observed in low concentration. The corresponding DMPO–OH spin adduct (*) consists of four lines of 1:2:2:1 intensities (aN = aH = 15 G).[27,45] The third line pattern (#) could be related to the oxidation of the spin trap and/or the rapid decomposition of the DMPO–OH adduct.[27,46] These results confirm that the complexes would be reduced in the parasite with a subsequent participation in redox cycling processes

that would generate reactive oxygen species like the OH radical.

Cruzipain Inhibitory Activity

Cruzipain, the main *T. cruzi* cysteine protease, has been validated as a drug target, and certain compounds that include the thiosemicarbazone moiety have shown inhibitory effects on the activity of this enzyme.[32] Therefore, the most active palladium and platinum compounds, [MCl(L4)PTA], as well as the free ligand L4, were screened against the cruzipain enzyme at 10 μM. All assayed compounds showed low potency as cruzipain inhibitors (14.6 ± 2.4, 11.9 ± 0.1, and 28.8 ± 1.5 percent inhibition for L4, [MCl(L4)PTA], and [MCl(L4)PTA], respectively). In spite of these low rates, the platinum complex, being the most active against *T. cruzi*, showed the best inhibitory effect on cruzipain.

DNA Interaction

The effect of all [MCl(L)(PTA)] complexes on plasmid DNA was determined by gel electrophoresis by using different r_i values at 37 °C during a 24 h incubation. The results are presented in Figure 6. The plasmid DNA used exhibited two main bands corresponding to the supercoiled form (higher mobility, Form I) and the circular relaxed DNA form (lower mobility, Form II). Between them, faint bands of intermediate mobility corresponding to different linking number topoisomers could be detected. The corresponding plasmid DNA linear form, which should also appear between the supercoiled and circular relaxed forms, was indistinguishable. Palladium and platinum complexes showed a different behavior, and differences were also observed within each series of metal complexes. While no obvious effect was exerted by [PdCl(L4)(PTA)], clear dose-dependent changes of the plasmid DNA migration pattern

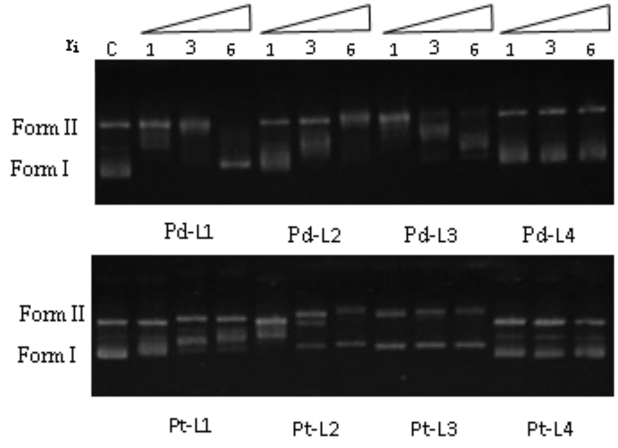

Figure 6. Interaction of plasmid DNA with [MCl(L)(PTA)] complexes. The different complexes studied are indicated at the bottom of each gel section. All reactions were incubated in 10 mM tris–HCl and 0.1 mM EDTA pH 7.4 in a final volume of 20 μL for 24 h at 37 °C. C indicates the control, which is plasmid DNA incubated at 37 °C for 24 h. Form I: pBR 322 supercoiled DNA; Form II: pBR 322 circular DNA. The variable r_i indicates the molar ratio of metal complex to DNA base pairs. Electrophoresis was carried out in the absence of ethidium bromide (EB). The gel was stained after the run.

were observed for the other three Pd^{2+} complexes, which supports the assumption of conformational changes. The interaction of these complexes with the plasmid DNA led to a decrease in the mobility of the supercoiled form, which is consistent with an intercalation-like activity.[19,47,48] For [PdCl(L2)(PTA)], a gradual loss of the plasmid negative supercoils accompanying the increasing r_i was observed. Indeed, the maximum assayed r_i yielded an almost complete loss of the plasmid DNA superhelicity. Meanwhile, such loss of superhelicity was observed for [PdCl(L1)(PTA)] and [PdCl(L3)(PTA)] complexes at lower r_i. Furthermore, for these two complexes, a plasmid DNA rewinding with positive supercoils was observed at increasing r_i. The reduced intensity or almost disappearance of the circular relaxed form, observed for the higher r_i values for these complexes, together with a subtle smear, put in evidence the existence of DNA degradation for the higher assayed r_i values.

Similarly to the performance of the palladium–L4 complex, the [PtCl(L4)(PTA)] complex had no effect on plasmid DNA migration. Incubation with [PtCl(L1)(PTA)] produced a dose-dependent shift of the plasmid DNA supercoiled form to lower migrations. For this complex, no induction of positive DNA supercoils was evident for the tested r_i. Instead, for [PtCl(L2)(PTA)] a gradual loss of negative and further appearance of positive supercoils was observed. A similar behavior was observed for [PtCl(L3)(PTA)], but for this complex the complete relaxation of negative supercoils is achieved at lower r_i values ($r_i < 1$) (Figure 6). It is interesting to mention that, for platinum complexes exhibiting an effect on plasmid DNA migration, a dose-dependent migration shift of the plasmid DNA forms relative to the control was observed.

Both DNA and [MCl(L)(PTA)] complexes are not fluorescent at pH = 7.4 in 10 mM TRIS/2%DMSO, and no fluorescence emission results from their direct interaction with DNA. As such, the well-established fluorescent DNA probe ethidium bromide (EB) was used to assess their interaction with DNA. Ethidium bromide (EB) is a conjugate planar molecule with weak intrinsic fluorescence emission at the appropriate excitation wavelengths, and at pH 7.4 in Tris buffer/2%DMSO, its spectrum shows an emission maximum at 601 nm ($\lambda_{exc.}$ = 510 nm). The binding of EB to DNA induces an increase of the fluorescence quantum yield when it is specifically intercalated into double-stranded DNA,[49,50] and in the spectrum of the {DNA-EB} adduct the emission maximum is shifted to 594 nm under our experimental conditions. The results obtained for the titration of the {DNA-EB} adduct with the complexes are summarized in Figures 7 and 8. As a general trend, a quenching of the emission of {DNA-EB} is observed upon increasing complex concentration (Figure 7), the extent of the quenching being quite different and dependent on the identity of the metal ion in the coordination complex (Figure 8). This indicates that all complexes tested interact with DNA with different affinities.

For the Pd complexes, very strong quenching of the fluorescence of {DNA-EB} was observed in a dose-dependent manner, with the exception of complex [PdCl(L4)(PTA)],

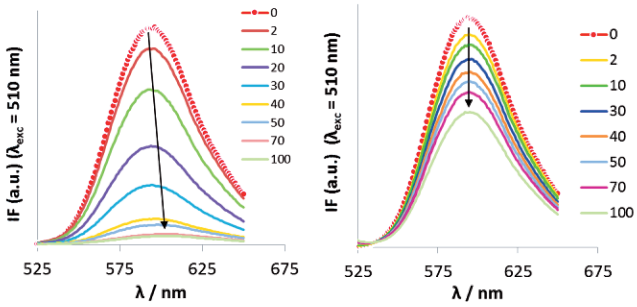

Figure 7. Steady-state fluorescence data obtained for the competitive binding of Pd and Pt complexes to {EB-DNA}. Left: fluorescence emission quenching ($\lambda_{exc.}$ = 510 nm) observed upon binding of complex [PdCl(L2)(PTA)]; similar results were obtained for all Pt complexes. Right: fluorescence emission quenching ($\lambda_{exc.}$ = 510 nm) observed upon binding of complex [PtCl(L4)(PTA)]; no shift in the $\lambda_{em.}^{max}$ is observed at the concentrations assayed. Similar results were obtained for all Pt complexes. (C_{DNA} = 20 μM, C_{EB} = 10 μM, samples prepared in 2%DMSO/TRIS HCl medium).

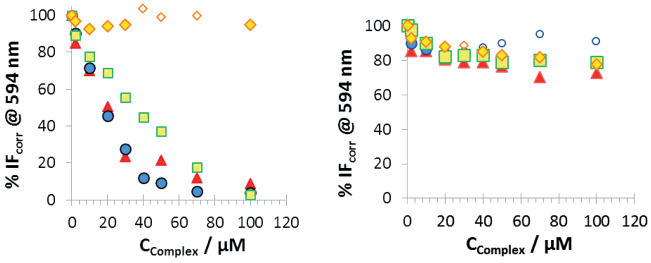

Figure 8. Relative fluorescence intensity (%) at $\lambda_{em.}$ = 594 nm with increasing complex concentration obtained for Pd complexes (left) and Pt complexes (right). (C_{DNA} = 20 μM, C_{EB} = 10 μM, samples prepared in 2%DMSO/TRIS HCl medium, 30 min incubation at 37 °C). Triangles: L1 complexes, circles: L2 complexes, squares: L3 complexes, and diamonds: L4 complexes.

which exhibited only a very slight effect on the emission intensity (ca. 5% quenching overall). Figure 7 depicts emission spectra recorded for {DNA-EB} with increasing concentrations of [PdCl(L2)(PTA)]. At high complex concentration (> 50 μM), the decrease in emission intensity was accompanied by an increasing red shift of 7 nm at 100 μM, changing the $\lambda_{max.}$ from 594 nm (characteristic of the {DNA-EB} adduct) to 601 nm (characteristic of the free EB spectrum). Similar results were observed for [PdCl(L1)(PTA)] and [PdCl(L2)(PTA)] complexes, with the relative intensity decreasing to ca. 4% for the first one or ca. 2.5% for the other. Figure 8 shows the extent to which the fluorescence emission was quenched in each case. These results are consistent with an EB displacement from the {DNA-EB} adduct brought upon by the complex, and the concomitant formation of a nonemissive {DNA complex} species, suggesting that the Pd complexes bind DNA in an intercalative-like manner and completely displace EB from DNA. However, another explanation can be envisaged: Pd complexes interact with DNA by inducing conformational changes, which cause the disruption of EB binding sites, thus promoting the release of the weakly fluorescent free EB molecules. On the other hand, results from gel electrophoresis experiments indicate that these complexes induce conformational changes in DNA, especially at high complex concentrations, ultimately resulting in degradation of the biopolymer chain. These observations suggest that, at high complex concentrations, disruption of the EB binding sites is taking place in solution upon the action of the Pd complexes, which form a nonemissive adduct with DNA.

For the Pt complexes, the formation of a DNA–complex adduct is detected by the moderate quenching observed of the {DNA-EB} fluorescence, with a maximum decrease to 70% of the initial intensity recorded for [PtCl(L1)(PTA)].

The mechanisms involved in the fluorescence quenching process for Pd and Pt complexes can be assessed by a Stern–Volmer analysis according to Equation (1).

$$I_{F0}/I_F = 1 + K_{SV}[Q] \quad (1)$$

In Equation (1), I_{F0} and I_F are the emission fluorescence intensity of the {DNA-EB} adduct in the absence and in the presence of the complex, respectively, K_{SV} is the Stern–Volmer constant, and [Q] is the concentration of the quencher (in this case, the complexes).[51] Equation (1) predicts a linear plot of I_{F0}/I_F for a homogeneously emitting system, but positive and negative deviations can be observed in some systems. Stern–Volmer analysis for the Pd and Pt complexes showed deviations from the linearity, positive for the Pd complexes and negative for the Pt complexes. Positive deviations of the Stern–Volmer plot are detected as a curve upward and are frequently observed when the extent of quenching is large. That is the case for the Pd complexes. In the low complex concentration range (typically up to 30 μM), the plot of I_{F0}/I_F is linear, and the K_{SV} constant can be calculated for these systems (Table 6). In the high-concentration range, gel electrophoresis experiments show that DNA is degraded by the action of these agents.

Table 6. Stern–Volmer constants obtained for [MCl(L)(PTA)] systems for the competitive binding to DNA-EB in 2%DMSO/TRIS HCl medium.

Complex		K_{SV} [M^{-1}]	log K_{SV}
Stern–Volmer plot			
[PdCl(L1)(PTA)]		46276	4.7
[PdCl(L2)(PTA)]		129569	5.1
[PdCl(L3)(PTA)]		25639	4.4
[PdCl(TF)(PTA)]		7267	3.9
	f_a	K_{SVa} [M^{-1}]	log K_{SVa}
Modified Stern–Volmer plot			
[PtCl(L1)(PTA)]	0.288	8512	3.9
[PtCl(L2)(PTA)]	0.161	22133	4.3
[PtCl(L3)(PTA)]	0.303	4079	3.6
[PtCl(TF)(PTA)]	0.207	3511	3.5

A Stern–Volmer plot that curves downward towards the x-axis is a characteristic feature of two fluorophore populations, one of which is not accessible to the quencher.[51] In

this case, the observed fluorescence intensity obeys Equation (2).

$$I_{F0}/\Delta I_F = 1/f_a K_{SVa}[Q] + 1/f_a \quad (2)$$

In Equation (2), $\Delta I_F = I_{F0} - I_F$, the subscript 0 referring to the fluorescence intensity in the absence of quencher, and $I_{F0} = I_{F0a} + I_{F0b}$ (*a* and *b* denoting the fluorophore fractions accessible and inaccessible, respectively). K_{SVa} is the Stern–Volmer quenching constant for the accessible fraction, $f_a = \frac{I_{F0a}}{I_{F0a} + I_{F0b}}$ is the fraction of the initial fluorescence accessible to the quencher, and [*Q*] is the concentration of the quencher. A plot of $\frac{I_{F0}}{\Delta I_F}$ versus $[Q]^{-1}$ yields f_a^{-1} as the intercept and $(f_a K_{SVa})^{-1}$ as the slope. K_{SVa} values obtained for the Pt complexes are summarized in Table 6.

Conclusions

In the search for potential antiparasitic metal complexes, eight new palladium(II) and platinum(II) complexes of formula [M(L)(PTA)] with 5-nitrofuryl-containing thiosemicarbazones as bioactive ligand and PTA (1,3,5-triaza-7-phosphaadamantane) as co-ligand were obtained. In these complexes, a square-planar coordination environment is proposed in which L acts as a bidentate monoanionic ligand through the imine nitrogen and the thiocarbonyl sulfur atoms. The studies on the equilibrium geometry conducted with B3LYP/LANL2DZ indicated the isomer with chloride *trans* to the sulfur donor atom to be the most stable one, regardless of the metal ion. PBE1PBE in combination with STMIDI could be confidently employed in studying metric parameters as well as infrared spectra of these complexes while keeping the computational cost very low. Most complexes showed activities against *T. cruzi* similar to those of the corresponding free thiosemicarbazone ligands. No significant differences between palladium and platinum complexes were observed. Metal compounds with the phenylthiosemicarbazone derivative were the most active ones. In addition, these complexes were not toxic to mammalian cells, showing high selective indexes. Related to the mechanism of action, the obtained compounds were able to produce toxic free radical species in the parasite. Even though cruzipain inhibition was low, it could not be completely discarded as the potential mechanism of action. On the other hand, both gel electrophoresis and EB fluorescence experiments are consistent with an intercalating-like mode of DNA interaction. However, the identity of the metal ion seems to determine the complex overall interaction with DNA. In fact, all Pd complexes show a much higher affinity for DNA in the EB displacement reaction and gel electrophoresis experiments than their Pt counterparts. Indeed, some palladium complexes produce DNA degradation at high DNA/complex molar ratios. In addition, fluorescence measurements indicate a different mechanism for the binding of the two sets of complexes. However, DNA interaction does not seem to be the main mechanism of anti *T. cruzi* action for these compounds. Both palladium and platinum [MCl(L)(PTA)] complexes show the least extent of DNA interaction of all the obtained complexes in spite of being the most active ones against *T. cruzi*.

Experimental Section

Materials: All common laboratory chemicals were purchased from commercial sources and used without further purification. PTA (1,3,5-triaza-7-phosphaadamantane), $Na_2[PdCl_4]$, and $K_2[PtCl_4]$ were purchased from Sigma–Aldrich. All 5-nitrofuryl-containing thiosemicarbazones were synthesized by using the previously reported methodology.[31]

Synthesis of [MCl(L)(PTA)] Complexes: $Na_2[PdCl_4]$ (25 mg, 0.08 mmol) or $K_2[PtCl_4]$ (35 mg, 0.08 mmol) and PTA (25 mg, 0.16 mmol) was dissolved in methanol (5 mL) by mixing and heating until complete dissolution. Then, the corresponding thiosemicarbazone ligand (0.08 mmol) was added to the solution. The mixture was heated at reflux for 24 h. The obtained solid was filtered off and washed with diethyl ether.

[PdCl(L1)(PTA)]: Yield: 22 mg, 52%. $C_{12}H_{17}ClN_7O_3PPdS$ (512.20): calcd. C 27.6, H 3.5, N 18.5, S 6.0; found C 28.1, H 3.1, N 19.1, S 6.2. ^{1}H NMR ([D$_6$]DMSO): δ = 7.94 (br, 3 H, C*H*=N + NH_2), 7.87 (m, 2 H, furan-H), 4.55 (d, 3 H, N–CH_2–N), 4.36 (d, 3 H, N–CH_2–N), 4.34 (s, 6 H, P–CH_2–N) ppm. ^{31}P{^{1}H} NMR ([D$_6$]-DMSO): δ = –27.8 (1 P, PTA) ppm. IR: $\tilde{\nu}$ = 1632 ν(C=N), 1326 $\nu_s(NO_2)$, 1166 ν(N–N), 808 [$\delta(NO_2)$ + furan] cm^{-1}.

[PdCl(L2)(PTA)]: Yield: 22 mg, 49%. $C_{13}H_{19}ClN_7O_3PPdS$ (526.22): calcd. C 29.6, H 3.9, N 17.7, S 6.1; found C 29.7, H 3.4, N 18.6, S 6.1. ^{1}H NMR ([D$_6$]DMSO): δ = 7.56 (d, 1 H, furan-*H*), 7.80 (d, 1 H, furan-*H*), 8.05 (br. d, 1 H, C*H*=N), 8.30 (d, 1 H, N*H*–CH_3), 2.91 (d, 3 H, CH_3), 4.55 (d, 3 H, N–CH_2–N), 4.37 (d, 3 H, N–CH_2–N), 4.35 (s, 6 H, P–CH_2–N) ppm. ^{31}P{^{1}H} NMR ([D$_6$]-DMSO): δ = –27.4 (1 P, PTA) ppm. IR: $\tilde{\nu}$ = 1587 ν(C=N), 1350 $\nu_s(NO_2)$, 1165 ν(N–N), 809 [$\delta(NO_2)$ + furan] cm^{-1}.

[PdCl(L3)(PTA)]: Yield: 32 mg, 70%. $C_{14}H_{21}ClN_7O_3PPdS$ (540.25): calcd. C 31.2, H 4.0, N 17.8, S 5.7; found C 31.2, H 3.7, N 18.2, S 5.9. ^{1}H NMR ([D$_6$]DMSO): δ = 7.52 (d, 1 H, furan-H), 7.79 (d, 1 H, furan-H), 8.05 (br. d, 1 H, C*H*=N), 8.34 (br, 1 H, N*H*–CH_2CH_3), 1.15 (t, 3 H, CH_3), 3.35 [m (overlapped with water, 3 H, CH_2)], 4.55 (d, 3 H, N–CH_2–N), 4.36 (d, 3 H, N–CH_2–N), 4.34 (s, 6 H, P–CH_2–N) ppm. ^{31}P{^{1}H} NMR ([D$_6$]DMSO): δ = –27.5 (1 P, PTA) ppm. IR: $\tilde{\nu}$ = 1562 ν(C=N), 1347 $\nu_s(NO_2)$, 1177 ν(N–N), 811 [$\delta(NO_2)$ + furan] cm^{-1}.

[PdCl(L4)(PTA)]: Yield: 39 mg, 78%. $C_{18}H_{21}ClN_7O_3PPdS$ (588.30): calcd. C 36.6, H 3.6, N 16.3, S 5.2; found C 36.9, H 3.4, N 16.7, S 5.5. ^{1}H NMR ([D$_6$]DMSO): δ = 7.63 (d, 1 H, furan-H), 7.79 (d, 1 H, furan-H), 8.15 (d, 1 H, C*H*=N), 10.29 (s, 1 H, N*H*-phenyl), 7.12 (t, 1 H, *p*-phenyl ring) 7.37 (t, 2 H, *m*-phenyl ring), 7.54 (2 H, *o*-phenyl ring), 4.57 (d, 3 H, N–CH_2–N), 4.38 (d, 3 H, N–CH_2–N), 4.39 (s, 6 H, P–CH_2–N) ppm. ^{31}P{^{1}H} NMR ([D$_6$]-DMSO): δ = –27.4 (1 P, PTA) ppm. IR: $\tilde{\nu}$ = 1597 ν(C=N), 1346 $\nu_s(NO_2)$, 1209 ν(N–N), 805 [$\delta(NO_2)$ + furan] cm^{-1}.

[PtCl(L1)(PTA)]: Yield: 29 mg, 57%. $C_{12}H_{17}ClN_7O_3PPtS$ (600.89): calcd. C 24.1, H 3.0, N 16.0, S 5.3; found C 24.0, H 2.7, N 16.3, S 5.3. ^{1}H NMR ([D$_6$]DMSO): δ = 7.89 (d, 1 H, furan-*H*), 7.97 (d, 1 H, furan-*H*), 8.21 (d, 1 H, C*H*=N), 8.11 (br, 2 H, NH_2), 4.48 (d, 3 H, N–CH_2–N), 4.39 (d, 3 H, N–CH_2–N), 4.23 (s, 6 H, P–CH_2–N) ppm. ^{31}P{^{1}H} NMR ([D$_6$]DMSO): δ = –60.0 (^{1}*J*P–Pt: = 3205 Hz,

1 P, PTA) ppm. IR: $\tilde{\nu}$ = 1536 ν(C=N), 1350 $\nu_s(NO_2)$, 1165 ν(N–N), 809 [$\delta(NO_2)$ + furan] cm^{-1}.

[PtCl(L2)(PTA)]: Yield: 17 mg, 33%. $C_{13}H_{19}ClN_7O_3PPtS$ (614.91): calcd. C 24.8, H 3.0, N 15.1, S 5.1; found C 25.4, H 2.9, N 15.9, S 5.2. ^{1}H NMR ([D$_6$]DMSO): δ = 7.62 (d, 1 H, furan-*H*), 7.81 (d, 1 H, furan-*H*), 8.34 (br, 1 H, C*H*=N), 8.42 (br, 1 H, N*H*–CH_3), 2.96 (d, 3 H, CH_3), 4.50 (d, 3 H, N–CH_2–N), 4.39 (d, 3 H, N–CH_2–N), 4.24 (s, 6 H, P–CH_2–N) ppm. ^{31}P{^{1}H} NMR ([D$_6$]DMSO): δ = –59.9 (^1JP–Pt: = 3208 Hz, 1 P, PTA) ppm. IR: $\tilde{\nu}$ = 1560 ν(C=N), 1340 $\nu_s(NO_2)$, 1162 ν(N–N), 812 [$\delta(NO_2)$ + furan] cm^{-1}.

[PtCl(L3)(PTA)]: Yield: 27 mg, 51%. $C_{14}H_{21}ClN_7O_3PPtS$ (628.94): calcd. C 26.7, H 3.4, N 15.2, S 4.9; found C 26.7, H 3.2, N 15.6, S 5.1. ^{1}H NMR ([D$_6$]DMSO): δ = 7.60 (d, 1 H, furan-H), 7.81 (d, 1 H, furan-H), 8.32 (br. d, 1 H, C*H*=N), 8.45 (br, 1 H, N*H*–CH_2CH_3), 1.16 (t, 3 H, CH_3), 3.39 (m, 2 H, CH_2), 4.49 (d, 3 H, N–CH_2–N), 4.39 (d, 3 H, N–CH_2–N), 4.24 (s, 6 H, P–CH_2–N) ppm. ^{31}P{^{1}H} NMR ([D$_6$]DMSO): δ = –59.9 (^1JP–Pt: = 3220 Hz, 1 P, PTA) ppm. IR: $\tilde{\nu}$ = 1562 ν(C=N), 1348 $\nu_s(NO_2)$, 1134 ν(N–N), 812 [$\delta(NO_2)$ + furan] cm^{-1}.

[PtCl(L4)(PTA)]: Yield: 24 mg, 42%. $C_{18}H_{21}ClN_7O_3PPtS$ (676.99): calcd. C 30.9, H 3.0, N 13.7, S 4.4; found C 31.9, H 3.0, N 14.5, S 4.7. ^{1}H NMR ([D$_6$]DMSO): δ = 7.72 (d, 1 H, furan-H), 7.83 (d, 1 H, furan-H), 8.40 (d, 1 H, C*H*=N), 10.45 (s, 1 H, N*H*-phenyl), 7.14 (t, 1 H, *p*-phenyl ring) 7.39 (t, 2 H, *m*-phenyl ring), 7.52 (2 H, *o*-phenyl ring), 4.50 (d, 3 H, N–CH_2–N), 4.40 (d, 3 H, N–CH_2–N), 4.27 (s, 6 H, P–CH_2–N) ppm. ^{31}P{^{1}H} NMR ([D$_6$]DMSO): δ = –59.5 (^1JP–Pt: = 3201 Hz, 1 P, PTA) ppm. IR: $\tilde{\nu}$ = 1596 ν(C=N), 1350 $\nu_s(NO_2)$, 1179 ν(N–N), 808 [$\delta(NO_2)$ + furan] cm^{-1}.

Physicochemical Characterization: C, H, N, and S analyses were performed with a Thermo Scientific Flash 2000 elemental analyzer. Conductivity measurements were performed at 25 °C in 1 mM water solutions using a Conductivity Meter 4310 Jenway. FTIR spectra (4000–400 cm^{-1}) of the complexes and the free ligands were measured with use of KBr pellets with a Bomen FTIR model M102 instrument. Electronic spectra were recorded with a Spectronic 3000 spectrophotometer. 1D and 2D NMR spectra were recorded with a Bruker Avance 400 MHz spectrometer (400.133 MHz for **^{1}H**, 160.984 MHz for **^{31}P**, 100.624 MHz for ^{13}C) equipped with a 5 mm multinuclear broad-band dual probe head, incorporating a z-gradient coil. Reported chemical shifts (in ppm) were measured in [D$_6$]DMSO at 296 K. The ^{1}H NMR spectra were calibrated with respect to the residual protonated signal of the solvent ([D$_6$]DMSO, 2.50 ppm to ^{1}H and 39.52 ppm to ^{13}C) and reported relative to Me_4Si. ^{31}P{^{1}H} NMR spectra were calibrated with respect to the external pattern H_3PO_4 10% (δ = 0.0 ppm). The electrochemical behavior was studied by cyclic voltammetry. Cyclic voltammograms were obtained with an Epsilon Electrochemical Analyzer. A standard electrochemical three-electrode cell of 10 mL volume completed the system. A hanging drop mercury electrode (HDME) was employed as working electrode. A platinum wire was used as counter electrode, while a Ag/Ag^+ electrode was used as reference electrode. Measurements were performed at room temperature in 1 mM DMSO solutions of the complexes by using tetrabutyl ammonium hexafluorophosphate (ca. 0.1 M) as supporting electrolyte. Solutions were deoxygenated by purging with nitrogen for 15 min prior to the measurements. A continuous gas stream was passed over the solution during the measurements. ESR spectra were recorded in the X band (9.85 GHz) with a Bruker ECS 106 spectrometer with a rectangular cavity and 50 kHz field modulation. The hyperfine splitting constants were estimated to be accurate within 0.05 G. The nitroanion radicals were generated by electrolytic reduction in situ under the same conditions of temperature, atmosphere, and concentrations stated for the CV experiment. The ESR spectra were simulated with the program WINEPR Simfonia (version 1.25).

Computational Details: All computational studies have been performed at the density functional level of theory (DFT). The geometry of the complexes was optimized in a closed-shell singlet (S = 1). The absence of crystallographic data prompted us to conduct stability studies of the isomers derived from the different coordination positions of chloride. No particular conformer has been considered. Their optimizations were conducted with B3LYP[52] in combination with LANL2DZ.[52,53] To shed light into the isomer composition of title complexes in the solid state, studies on equilibrium geometry were performed by employing PBE1PBE[54] in combination with the so-called STMIDI basis set (see below for details). The complex [PtCl(L3)(PTA)] has been taken into account as example. PBE1PBE/STMIDI has proved to adequately describe geometries of large complexes[38–42] with a very low computational cost. The valence electrons for nonmetal atoms in STMIDI were treated with MIDI!,[55] those for the metal being described by a basis set (8s7p6d2f1g)/[6s5p3d2f1g].[56] The core electrons were replaced by Stuttgart effective-core pseudopotentials.[56,57] LANL2DZ and STMIDI take scalar relativistic effects into account, which are especially important when systems with heavy atoms are studied.[58] The nature of the stationary point was verified through a vibrational analysis (no imaginary frequencies). All theoretical studies reported in this work were conducted by employing the program package Gaussian 09, Rev. A.01.[59]

Lipophilicity: Lipophilicity was studied by reversed-phase TLC experiments performed on precoated TLC plates SIL RP-18W/UV254 and eluted with DMSO/physiological serum (60:40 v/v). Stock solutions were prepared in pure acetone prior to use. The plates were developed in a closed chromatographic tank and dried, and the spots were located under UV light. The R_f values were averaged from three determinations and converted into R_M values by the relationship: $R_M = \log[(1/R_f) - 1]$.[21,27]

Viability on *T. cruzi* (Dm28c clone) Trypomastigotes: Vero cells were infected with *T. cruzi* metacyclic trypomastigotes from 15 d old Dm28c clone epimastigote cultures. Subsequently, the trypomastigotes harvested from this culture were used to infect further Vero cell cultures at a density of 1×10^6 parasites per 25 cm^3. These trypomastigote-infected Vero cell cultures were incubated at 37 °C in humidified air and 5% CO_2 for 5 to 7 d. After this time, culture media were collected and centrifuged at 3,000 × g for 5 min. The trypomastigote-containing pellets were resuspended in Roswell Park Memorial Institute Media (RPMI) supplemented with 5% fetal bovine serum and penicillin–streptomycin at a final density of 1×10^7 parasites/mL. 210×10^6 trypomastigotes are equivalent to 1 mg of protein or 12 mg of wet weight. Viability assays were performed by using the MTT [3-(4,5-dimethylthiazol-2-yl)-2,5-diphenyltetrazolium bromide] reduction method as described previously.[60,61] Briefly, 1×10^7 trypomastigotes were incubated in fetal bovine serum–RPMI culture medium at 37 °C for 24 h with and without the complexes under study at final concentrations of 5 to 100 μM. An aliquot of the parasite suspension was extracted and it was incubated in a flat-bottom 96-well plate. MTT was added at a final concentration of 0.5 mg/mL, incubated at 28 °C for 4 h, and then solubilized with 10% sodium dodecyl sulfate 0.1 mM HCl and incubated overnight. Formazan formation was measured at 570 nm with the reference wavelength at 690 nm in a multiwell reader (Labsystems Multiskan MS). Untreated parasites were used as negative controls (100% of viability). Finally, a nonlinear regression analysis, by using the fit of log(concentration) against normalized response, was performed with Graph Pad prism software.

Cytotoxicity on Mammalian Cells: The endothelial cell lines EA.hy926 [permanent human cell line derived by fusing human umbilical vein endothelial cells (HUVEC) with human lung cells (A549)] were maintained in the nutrient medium Iscove's Modified Dulbecco's Medium (IMDM) (Sigma–Aldrich), which was supplemented with 10% fetal bovine serum, (25 mM), penicillin (100 units/mL), and streptomycin (100 mg/mL). The cells were maintained as a monolayer culture in tissue culture flasks (Thermo Scientific Nunc™) in an incubator at 37 °C in a humidified atmosphere composed of 5% CO_2. Viability assays were performed by using the MTT reduction method as described previously for *T. cruzi* trypomastigote assay (see above).

Generation of Free Radical Species in *T. cruzi*: The free radical production capacity of the new complexes was assessed in the parasite with ESR spectroscopy by using DMPO for spin trapping. Each tested compound was dissolved in DMSO (spectroscopy grade, approx. 1 mM), and the solution was added to a mixture containing the epimastigote form of *T. cruzi* (Dm28c strain; final protein concentration, 4–8 mg/mL) and DMPO (final concentration, 250 mM). The mixture was transferred to a 50-μL capillary. ESR spectra were recorded in the X band (9.85 GHz) by using a Bruker ECS 106 spectrometer with a rectangular cavity and 50-kHz field modulation. All the spectra were registered in the same scale, after 15 scans.[31]

Cruzipain Inhibitory Activity: Cruzipain was purified to homogeneity from epimastigotes of the Tulahuen 2 strain.[62] Cruzipain (2.6 nM) was incubated in 50 mM Tris–HCl (pH 7.6). Then, the chromogenic substrate N-Benzoyl-Pro-Phen-Arg-pNA was added to give 3 mM substrate. Changes in absorbance intensity were registered for 5 min at emission wavelengths of 410 nm. The final assay volume was 200 μL with a DMSO concentration of 0.5%. At this concentration, DMSO did not significantly affect the activity of cruzipain. Stock solutions (10 mM) of the complexes were prepared in DMSO and screened at 10 μM. Controls were performed with the enzyme dissolved in DMSO. The percentage of cruzipain inhibition (*CI*) was calculated as follows: $CI\ (\%) = (v_i/v_o) \times 100$, where v_i and v_o correspond to the Δ(absorbance)/minute, with and without inhibitor, respectively.

Gel Electrophoresis Approach: Experiments of the interaction with plasmid DNA were performed by a previously described procedure but using commercial plasmid DNA (pBR322, ROCHE).[19] Metal complexes were dissolved in DMSO/water (25% v/v). No effect on DNA was observed due to the addition of DMSO (percentage of DMSO in the incubation mixture: 6.25). Plasmid DNA (200 ng) was incubated with the metal complexes for 24 h at 37 °C [final volume: 20 μL, reaction buffer: Tris 10mM, EDTA (ethylenediaminetetraacetic acid disodium salt) 0.1 mM, pH 7.4]. Various molar ratios (r_i is the mol ratio of complex to DNA base pair) were assayed. After incubation, reactions were stopped by adding loading buffer (25% bromophenol blue, 50% glycerol, 25 mM EDTA pH 8.0). In all cases, samples were electrophoresed in 0.7% agarose buffered with TBE (90 mM Tris–borate, 2 mM EDTA) at pH 8 at 70–80 V for 2 h. The gel was subsequently stained with an ethidium bromide solution (0.5 μg/mL) for 30 min and destained in water for 20 min. Bands were visualized under UV light.

Fluorescence Studies: Experiments for competitive binding to calf thymus DNA (ctDNA, SIGMA, Type I, No. D-1501) with ethidium bromide (EB, SIGMA) were carried out in 10 mM Tris-HCl buffer at pH 7.4. Millipore® water was used for the preparation of all aqueous solutions. Fluorescence measurements were carried out on individually prepared samples to ensure the same pre-incubation time for all samples in each assay. Due to the low solubility of the complexes in aqueous media, dimethyl sulfoxide (DMSO, Carlo Erba) was used to prepare concentrated stock solutions of each complex [MCl(L)(PTA)] (M = Pd or Pt) followed by appropriate dilution to obtain the targeted concentration and the same content of DMSO (5% v/v) in the final samples. DNA stock solutions were prepared by hydrating ctDNA in Tris-HCl buffer (1 mg/mL, ca. 2 mM nuc^{-1}) for 3–4 d at 4 °C, swirling the solution about 4–5 times a day until full dissolution was attained, and a clear solution was obtained. This solution was kept at 4 °C (in the fridge) in-between measurements and discarded after 4 d. The concentration of each stock solution was determined by UV spectrophotometry by using the molar extinction coefficient $\varepsilon(260\ nm) = 6600\ M^{-1}\ cm^{-1} nuc^{-1}$.[63] An EB 5 mM solution was prepared in Tris-HCl buffer. cDNA was pre-incubated with EB at 4 °C for 24 h. Samples were prepared with a total concentration of DNA and of EB of 20 μM nuc^{-1} and 10 μM, respectively, by varying the total complex concentration from 2 to 100 μM. They were incubated at 37 °C for 30 min. Samples with complex alone and samples with complex and EB but no DNA were used as blanks. Fluorescence spectra were recorded from 520 nm to 650 nm at an excitation wavelength of 510 nm with a Shimadzu RF-5301PC spectrofluorometer. Fluorescence emission intensity was corrected for the absorption and emission inner filter effect at the maximum emission wavelength (594 nm) by using the UV/Visible absorption data recorded for each sample according to Equation (3).[51]

$$I_{Fcorr} = I_F \times 10^{(Abs_{\lambda exc} + Abs_{\lambda em})/2} \quad (3)$$

Supporting Information (see footnote on the first page of this article): Tentatively assigned IR bands for the PTA ligand in the obtained complexes.

Acknowledgments

The authors wish to thank Agencia Nacional de Investigación e Innovación – Uruguay (ANII–Uruguay) (project FCE_2011_6963) and Fondecyt (11080166 and 1110029), as well as the International Cooperation Project, Chile for financial support. M. C. thanks Agencia Nacional de Investigación e Innovación – Uruguay (ANII–Uruguay) for research grant Be_INI_2010_2_3116. A. I. T. thanks the Portuguese Foundation for Science and Technology for project IF/01179/2013 and for the Investigador FCT Initiative.

[1] G. Sava, A. Bergamo, P. J. Dyson, *Dalton Trans.* **2011**, *40*, 9069–9075.
[2] S. Rafique, M. Idrees, A. Nasim, H. Akbar, A. Athar, *Biotechnol. Mol. Biol. Rev.* **2010**, *5*, 38–45.
[3] S. P. Fricker, *Dalton Trans.* **2007**, 4903–4917.
[4] L. Ronconi, P. J. Sadler, *Coord. Chem. Rev.* **2007**, *251*, 1633–1648.
[5] A. Garoufis, S. K. Hadjikakou, N. Hadjiliadis, *Coord. Chem. Rev.* **2009**, *253*, 1384–1397.
[6] M. Navarro, G. Gabbiani, L. Messori, D. Gambino, *Drug Discovery Today* **2010**, *15*, 1070–1077.
[7] D. Gambino, *Coord. Chem. Rev.* **2011**, *255*, 2193–2203.
[8] R. A. Sánchez-Delgado, A. Anzellotti, *Mini-Rev. Med. Chem.* **2004**, *4*, 22–30.
[9] M. Navarro, *Coord. Chem. Rev.* **2009**, *253*, 1619–1626.
[10] S. P. Fricker, R. M. Mosi, B. R. Cameron, I. Baird, Y. Zhu, V. Anastassov, J. Cox, P. S. Doyle, E. Hansell, G. Lau, J. Langille, M. Olsen, L. Qin, R. Skerlj, R. S. Y. Wong, Z. Santucci, J. H. McKerrow, *J. Inorg. Biochem.* **2008**, *102*, 1839–1845.
[11] D. Gambino, L. Otero, *Inorg. Chim. Acta* **2012**, *393*, 103–114.
[12] C. M. Beaumier, P. M. Gillespie, P. J. Hotez, M. E. Bottazzi, *Transl. Res.* **2013**, *162*, 144–155.

[13] B. Liese, M. Rosenberg, A. Schratz, *Lancet* **2010**, *375*, 67–76.
[14] F. Astelbauer, J. Walochnik, *Int. J. Antimicrob. Agents* **2011**, *38*, 118–124.
[15] A. Rassi Jr., A. Rassi, J. A. Marin-Neto, *Lancet* **2010**, *375*, 1388–1402.
[16] J. Rodrigues Coura, J. Borges-Pereira, *Acta Trop.* **2010**, *115*, 5–13.
[17] B. Demoro, M. Rossi, F. Caruso, D. Liebowitz, C. Olea-Azar, U. Kemmerling, J. D. Maya, H. Guiset, V. Moreno, C. Pizzo, G. Mahler, L. Otero, D. Gambino, *Biol. Trace Elem. Res.* **2013**, *153*, 371–381.
[18] B. Demoro, C. Sarniguet, R. Sánchez-Delgado, M. Rossi, D. Liebowitz, F. Caruso, C. Olea-Azar, V. Moreno, A. Medeiros, M. Comini, L. Otero, D. Gambino, *Dalton Trans.* **2012**, *41*, 1534–1543.
[19] M. Vieites, P. Smircich, M. Pagano, L. Otero, F. Luane, H. Terenzi, M. J. Prieto, V. Moreno, B. Garat, D. Gambino, *J. Inorg. Biochem.* **2011**, *105*, 1704–1711.
[20] A. Merlino, L. Otero, D. Gambino, E. L. Coitiño, *Eur. J. Med. Chem.* **2011**, *46*, 2639–2651.
[21] M. Pagano, B. Demoro, J. Toloza, L. Boiani, M. González, H. Cerecetto, C. Olea-Azar, E. Norambuena, D. Gambino, L. Otero, *Eur. J. Med. Chem.* **2009**, *44*, 4937–4943.
[22] M. Vieites, L. Otero, D. Santos, C. Olea-Azar, E. Norambuena, G. Aguirre, H. Cerecetto, M. González, U. Kemmerling, A. Morello, J. D. Maya, D. Gambino, *J. Inorg. Biochem.* **2009**, *103*, 411–418.
[23] M. Vieites, L. Otero, D. Santos, D. Gajardo, J. Toloza, R. Figueroa, E. Norambuena, C. Olea-Azar, G. Aguirre, H. Cerecetto, M. González, A. Morello, J. D. Maya, B. Garat, D. Gambino, *J. Inorg. Biochem.* **2008**, *102*, 1033–1043.
[24] L. Otero, J. D. Maya, A. Morello, C. Rigol, G. Barriga, J. Rodriguez, C. Folch, E. Norambuena, M. Gonzalez, C. Olea-Azar, H. Cerecetto, D. Gambino, *Medicinal Chemistry* **2008**, *4*, 11–17.
[25] L. Otero, C. Folch, G. Barriga, C. Rigol, L. Opazo, M. Vieites, D. Gambino, H. Cerecetto, E. Norambuena, C. Olea-Azar, *Spectrochim. Acta Part A* **2008**, *70*, 519–523.
[26] L. Otero, M. Vieites, L. Boiani, A. Denicola, C. Rigol, L. Opazo, C. Olea-Azar, J. D. Maya, A. Morello, L. Krauth-Siegel, O. E. Piro, E. Castellano, M. González, D. Gambino, H. Cerecetto, *J. Med. Chem.* **2006**, *49*, 3322–3331.
[27] C. Sarniguet, J. Toloza, M. Cipriani, M. Lapier, M. Vieites, Y. Toledano-Magaña, J. C. García-Ramos, L. Ruiz-Azuara, V. Virtudes Moreno, J. D. Maya, C. O. Azar, D. Gambino, L. Otero, *Biol. Trace Elem. Res.* **2014**, *159*, 379–392.
[28] N. P. Farrell, J. Williamson, D. J. M. McLaren, *Biochem. Pharmacol.* **1984**, 961–968.
[29] A. D. Phillips, L. Gonsalvi, A. Romerosa, F. Vizza, M. Peruzzini, *Coord. Chem. Rev.* **2004**, *248*, 955–993.
[30] J. Bravo, S. Bolaño, L. Gonsalvi, M. Peruzzini, *Coord. Chem. Rev.* **2010**, *254*, 555–607.
[31] G. Aguirre, H. Cerecetto, M. González, D. Gambino, L. Otero, C. Olea-Azar, C. Rigol, A. Denicola, *Bioorg. Med. Chem.* **2004**, *12*, 4885–4893.
[32] J. J. Cazzulo, *Curr. Top. Med. Chem.* **2002**, *2*, 1261–1271.
[33] D. Gambino, L. Otero, M. Vieites, M. Boiani, M. Gonzalez, E. J. Baran, H. Cerecetto, *Spectrochim. Acta Part A* **2007**, *68*, 341–348.
[34] K. Jogun, J. J. Stezowski, E. Fluck, J. Weidlein, *Phosphorus Sulfur Relat. Elem.* **1978**, *4*, 99–204.
[35] P. Chellan, T. Stringer, A. Shokar, P. J. Dornbush, G. Vazquez-Anaya, K. M. Land, K. Chibale, G. S. Smith, *J. Inorg. Biochem.* **2011**, *105*, 1562–1568.
[36] P. Smolenski, A. J. L. Pombeiro, *Dalton Trans.* **2008**, 87–91.
[37] A. Romerosa, P. Bergamini, V. Bertolasi, A. Canella, M. Cattabriga, R. Gavioli, S. Mañas, N. Mantovani, L. Pellacani, *Inorg. Chem.* **2004**, *43*, 905–913.
[38] L. Martínez, J. S. Gancheff, F. E. Hahn, R. A. Burrow, R. González, C. Kremer, R. Chiozzone, *Spectrochim. Acta Part A* **2013**, *105*, 439–445.
[39] J. S. Gancheff, Á. Acosta, D. Armentano, G. De Munno, R. Chiozzone, R. González, *Inorg. Chim. Acta* **2012**, *387*, 314–320.
[40] C. Pejo, H. Pardo, A. Mombrú, M. F. Cerdá, J. S. Gancheff, R. Chiozzone, R. González, *Inorg. Chim. Acta* **2011**, *376*, 105–111.
[41] J. S. Gancheff, P. A. Denis, E. F. Hahn, *THEOCHEM* **2010**, *941*, 1–9.
[42] J. S. Gancheff, R. Q. Albuquerque, A. Guerrero-Martínez, T. Pape, L. De Cola, F. E. Hahn, *Eur. J. Inorg. Chem.* **2009**, 4043–4051.
[43] S. Day, L. B. Kumbhare, V. K. Jain, T. Schurr, W. Kaim, A. Klein, F. Belaj, *Eur. J. Inorg. Chem.* **2004**, 4510–4520.
[44] C. Rigol, C. Olea-Azar, F. Mendizabal, L. Otero, D. Gambino, M. Gonzalez, H. Cerecetto, *Spectrochim. Acta Part A* **2005**, *61*, 2933–2938.
[45] K. Makino, T. Hagiwara, A. Murakami, *Radiat. Phys. Chem.* **1991**, *37*, 657–665.
[46] B. Aguilera-Venegas, C. Olea-Azar, V. Arán, J. D. Maya, U. Kemmerling, H. Speisky, F. Mendizábal, *Int. J. Electrochem. Sci.* **2012**, *7*, 5837–5863.
[47] L. Otero, P. Smircich, M. Vieites, M. Ciganda, P. Cardoso Severino, H. Terenzi, H. Cerecetto, D. Gambino, B. Garat, *J. Inorg. Biochem.* **2007**, *101*, 74–79.
[48] K. Storl, G. Burckhardt, J. W. Lown, C. Zimmer, *FEBS Lett.* **1993**, *334*, 49–54.
[49] M. J. Waring, *J. Mol. Biol.* **1965**, *13*, 269–282.
[50] C. Tan, J. Liu, L. M. Chen, S. Shi, L. N. Ji, *J. Inorg. Biochem.* **2008**, *102*, 1644–1653.
[51] J. R. Lakowicz, *Principles of Fluorescence Spectroscopy*, 3rd. ed., Springer, New York, **2006**, ch. 8.
[52] a) A. D. Becke, *Phys. Rev. A* **1988**, *38*, 3098–3100; b) A. D. Becke, *J. Chem. Phys.* **1993**, *98*, 1372–1377; c) C. Lee, W. Yang, R. G. Parr, *Phys. Rev. B* **1988**, *37*, 785–789.
[53] a) P. J. Hay, W. R. Wadt, *J. Chem. Phys.* **1985**, *82*, 270–283; b) P. J. Hay, W. R. Wadt, *J. Chem. Phys.* **1985**, *82*, 284–298; c) P. J. Hay, W. R. Wadt, *J. Chem. Phys.* **1985**, *82*, 299–310.
[54] a) C. Adamo, V. Barone, *J. Chem. Phys.* **1999**, *110*, 6158–6170; b) J. P. Perdew, K. Burke, M. Ernzerhof, *Phys. Rev. Lett.* **1996**, *77*, 3865–3868; c) A. D. Becke, *J. Chem. Phys.* **1993**, *98*, 5648–5652.
[55] R. E. Easton, D. J. Giesen, A. Welch, C. J. Cramer, D. G. Truhlar, *Theor. Chim. Acta* **1996**, *93*, 281–301.
[56] a) M. Dolg, U. Wedig, H. Stoll, H. Preuss, *J. Chem. Phys.* **1987**, *86*, 866–872; b) J. M. L. Martin, A. Sundermann, *J. Chem. Phys.* **2001**, *114*, 3408–3420; c) D. Andrae, U. Häussermann, M. Dolg, H. Stoll, H. Preuss, *Theor. Chim. Acta* **1990**, *77*, 123–141.
[57] A. Bergner, M. Dolg, W. Kuechle, H. Stoll, M. Preuss, *Mol. Phys.* **1993**, *80*, 1431–1441.
[58] P. Pyykkö, *The Effect of Relativity in Atoms, Molecules and The Solid State*, Plenum, New York, **1990**.
[59] M. J. Frisch, G. W. Trucks, H. B. Schlegel, G. E. Scuseria, M. A. Robb, J. R. Cheeseman, G. Scalmani, V. Barone, B. Mennucci, G. A. Petersson, H. Nakatsuji, M. Caricato, X. Li, H. P. Hratchian, A. F. Izmaylov, J. Bloino, G. Zheng, J. L. Sonnenberg, M. Hada, M. Ehara, K. Toyota, R. Fukuda, J. Hasegawa, M. Ishida, T. Nakajima, Y. Honda, O. Kitao, H. Nakai, T. Vreven, J. A. Montgomery Jr., J. E. Peralta, F. Ogliaro, M. Bearpark, J. J. Heyd, E. Brothers, K. N. Kudin, V. N. Staroverov, R. Kobayashi, J. Normand, K. Raghavachari, A. Rendell, J. C. Burant, S. S. Iyengar, J. Tomasi, M. Cossi, N. Rega, J. M. Millam, M. Klene, J. E. Knox, J. B. Cross, V. Bakken, C. Adamo, J. Jaramillo, R. Gomperts, R. E. Stratmann, O. Yazyev, A. J. Austin, R. Cammi, C. Pomelli, J. W. Ochterski, R. L. Martin, K. Morokuma, V. G. Zakrzewski, G. A. Voth, P. Salvador, J. J. Dannenberg, S. Dapprich, A. D. Daniels, Ö. Farkas, J. B.

Foresman, J. V. Ortiz, J. Cioslowski, D. J. Fox, *Gaussian 09 Revision A.1*, Gaussian Inc., Wallingford CT, **2009**.
[60] S. Muelas-Serrano, J. J. Nogal-Ruiz, A. Gómez-Barrio, *Parasitol. Res.* **2002**, *86*, 999–1002.
[61] M. Faundez, L. Pino, P. Letelier, C. Ortiz, R. López, C. Seguel, J. Ferreira, M. Pavani, A. Morello, J. D. Maya, *Antimicrob. Agents Chemother.* **2005**, *49*, 126–130.
[62] F. Parussini, M. Garcia, J. Mucci, F. Aguero, D. Sanchez, U. Hellman, L. Aslund, J. J. Cazzulo, *Mol. Biochem. Parasitol.* **2003**, *131*, 11–23.
[63] J. K. Barton, J. M. Goldberg, Ch. V. Kumar, N. J. Turro, *J. Am. Chem. Soc.* **1986**, *108*, 2081–2088.

Received: July 1, 2014
Published Online: September 8, 2014

